Spin-wave instability in itinerant ferromagnets

Takuya Okabe
Department of Physics, Kyoto University, Kyoto 606-01, Japan
(Received 29 July 1997)

We show variationally that instability of the ferromagnetic state in the Hubbard model is largely controlled by softening of a long-wavelength spin-wave excitation, except in the overdoped strong-coupling region where the individual-particle excitation becomes unstable first. A similar conclusion is drawn also for the double-exchange ferromagnet. Generally the spin-wave instability may be regarded as a precursor of the metal-insulator transition. [S0163-1829(98)03601-7]

I. INTRODUCTION

Recently the electron correlation effect in the strong-coupling Hubbard model around half filling has been intensively investigated. Since Nagaoka showed the existence of the itinerant ferromagnetic ground state in the limit $U\to\infty$ and $n\to 1$,[1] several authors[2–7] attempted a variational estimate of the stability of the ferromagnetic state in this limit. On the other side, there are works that try to investigate the metal-insulator transition from the ferromagnetic side. In particular, the two-body problem of a particle-hole pair in the half-filled band was treated as an exactly solvable case of the Mott transition by several authors.[8–11] To describe physically relevant situations in this approach, one must treat the many-body problem of the particle-hole bound states. For example, one may use the BCS-type mean-field approximation when the ground state is magnetically ordered.[10,12,13]

In this paper we discuss the stability of the Nagaoka ferromagnetic state, with the problem of the metal-insulator transition in mind. We show that the ferromagnetic state in the over-doped region of the strong coupling Hubbard model is destabilized by the individual-particle excitation, as Shastry, Krishnamurthy, and Anderson noted.[4] However, it is found that in almost all the other regions the instability is controlled by softening of the spin-wave stiffness. In Sec. III A, we give a phase diagram showing this feature on the basis of a variational trial state. We estimate an upper bound for κ, which is defined by $\kappa\equiv zt/U_c x$ for the ferromagnetic threshold in the limit $U\to\infty$ and $x=1-n\to 0$. Stability of the double-exchange ferromagnet is discussed in Sec. III B. Incidentally, in Appendix A, we discuss that the antiferromagnetic Heisenberg model can be reproduced by using the results of the two-body problem, or from the spin wave in the insulating ferromagnetic state. Mathematical details are given in Appendix B.

II. VARIATIONAL DESCRIPTION OF THE SPIN-WAVE EXCITED STATE

A. Random phase approximation

We first investigate the ferromagnetic state,

$$|F\rangle\equiv\prod_{\varepsilon_k<\varepsilon_f} c_{k\uparrow}^{\dagger}|0\rangle, \tag{1}$$

of the Hubbard model,

$$H=-\sum_{i,j,\sigma} t_{ij}c_{i\sigma}^{\dagger}c_{j\sigma}+U\sum_i \hat{n}_{i\uparrow}\hat{n}_{i\downarrow}$$

$$=\sum_{k\sigma} \varepsilon_k c_{k\sigma}^{\dagger}c_{k\sigma}+U\sum_i \hat{n}_{i\uparrow}\hat{n}_{i\downarrow}. \tag{2}$$

By way of illustration, here we present results obtained in the random phase approximation (RPA) first. To this end, we may use the following trial state for the spin-wave excited state:

$$|\Psi_q\rangle=b_q^{\dagger}|F\rangle, \tag{3}$$

where

$$b_q^{\dagger}\equiv\frac{1}{\sqrt{L}}\sum_{i,j} f_q(r_j-r_i)c_{i\downarrow}^{\dagger}c_{j\uparrow}e^{iqr_i} \tag{4}$$

$$=\frac{1}{\sqrt{L}}\sum_k f_q(k)c_{k+q\downarrow}^{\dagger}c_{k\uparrow}, \tag{5}$$

and L denotes the total number of lattice sites. Then we obtain

$$\langle F|b_q[H,b_q^{\dagger}]|F\rangle=\frac{1}{L}\sum_k n_k(\varepsilon_{k+q}-\varepsilon_k+Un)|f_q(k)|^2$$

$$-U\left|\frac{1}{L}\sum_k n_k f_q(k)\right|^2, \tag{6}$$

$$\langle F|b_q b_q^{\dagger}|F\rangle=\frac{1}{L}\sum_k n_k|f_q(k)|^2, \tag{7}$$

where

$$n_k=\begin{cases}1, & \varepsilon_k<\varepsilon_f\\ 0, & \varepsilon_k>\varepsilon_f\end{cases} \tag{8}$$

and carrier density n is defined by

$$n\equiv\frac{1}{L}\sum_k \langle F|n_k|F\rangle.$$

Taking the functional derivative of

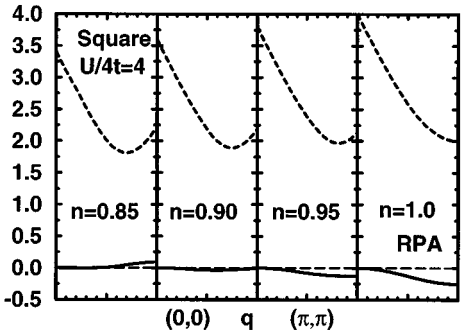

FIG. 1. Dispersion of the spin wave ($\omega_q/4t$) and the bottom of continuum [$\eta_{\min}(q)/4t$)] along (q,q) $(0\leqslant q\leqslant\pi)$ in the RPA.

$$\omega_q=\frac{\langle F|b_q[H,b_q^\dagger]|F\rangle}{\langle F|b_q b_q^\dagger|F\rangle}, \tag{9}$$

with respect to $f_q(k)$, we obtain

$$f_q(k)=\frac{1}{\varepsilon_{k+q}-\varepsilon_k+Un-\omega_q}\frac{U}{L}\sum_k n_k f_q(k). \tag{10}$$

Summing $n_k f_q(k)$ over k, we have the eigenequation

$$\frac{1}{L}\sum_k \frac{n_k}{\varepsilon_{k+q}-\varepsilon_k+Un-\omega_q}=\frac{1}{U}. \tag{11}$$

Substituting $f_q(k')=\delta_{kk'}$ in Eqs. (6), (7), and (9), we obtain

$$\eta_q(k)=\varepsilon_{k+q}-\varepsilon_k+Un \tag{12}$$

for the energy of the particle-hole continuum. The bound state (spin wave) energy ω_q is given as a solution of Eq. (11). In particular, for a tight-binding dispersion in a square lattice, the results are shown in Fig. 1 for $\mathbf{q}=(q,q)$ $(0\leqslant q\leqslant\pi)$ for various values of n. The spin-wave part of Fig. 1 is shown in Fig. 2. The result for $n=1$ reproduces the two-body result given in Appendix A. Discussion based on Eq. (11) is equivalent to the random phase approximation, which properly takes into account the two-body correlation effect of the particle-hole ladder. In all of the cases shown in the figures, the ferromagnetic state is unstable to the spin-wave excitation.

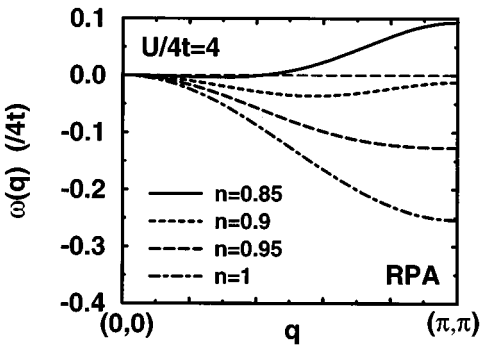

FIG. 2. Dispersion $\omega(q)$ for $U/4t=4$ in the RPA.

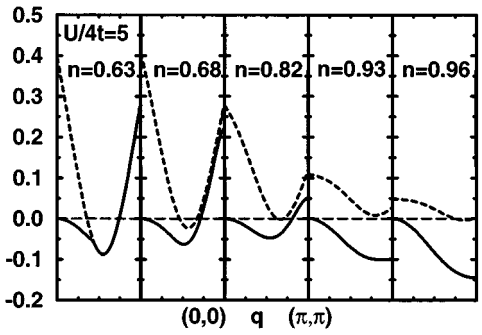

FIG. 3. Dispersion of the spin wave ($\omega_q/4t$) and the bottom of continuum [$\eta_{\min}(q)/4t$] along (q,q) $(0\leqslant q\leqslant\pi)$ calculated with the improved trial state.

From these results, we observe several points. (i) ω_q and $\eta_q(k)$ are separated by energy gap of order U (Fig. 1). (ii) The bandwidth of ω_q becomes narrow and (iii) the minimum of ω_q moves away from $\mathbf{q}=\mathbf{Q}=(\pi,\pi)$ as the density of holes increases (Fig. 2). For example, the minimum of ω_q for $U/4t=4$ and $n=0.9$ lies at $\mathbf{q}=(\pi,0.3\pi)$. With respect to (iii), we are led to the following speculation; beyond spin-wave instability, the spin wave with momentum $q=q_{\min}$ that gives the minimum $\omega_q\leqslant 0$ will be set to populate the ferromagnetic state, resulting in Bose-Einstein condensation of the boson $b_{q_{\min}}^\dagger$. In particular, around half filling $n\lesssim 1$, the resulting state will be the commensurate Néel ordered phase with $\mathbf{q}=\mathbf{Q}$. Upon doping $n\lesssim 0.93$, e.g., for $U/4t=4$, the resulting phase will become the spiral state with incommensurate modulation $\mathbf{q}\neq\mathbf{Q}$. Qualitatively this is consistent with the result of recent studies.[14–16] Moreover, further hole doping ($n\lesssim 0.82$ for $U/4t=4$) stabilizes the ferromagnetic state, just as concluded from the mean-field treatment.[15,16] However, the latter point on the stability of the ferromagnetic state as well as the above point (i) are shown to be modified by improving the approximation.

B. Improved trial state

Next we consider the following creation operator to improve the trial state created by Eq. (4):

$$b_q^\dagger\equiv\frac{1}{\sqrt{L}}\sum_{i,j} f_q(r_j-r_i)c_{i\downarrow}^\dagger(\sin\theta+\cos\theta c_{i\uparrow}c_{i\uparrow}^\dagger)c_{j\uparrow}e^{iqr_i}. \tag{13}$$

The wave function of this form was first used by Roth[2] and also adopted later by Shastry, Krishnamurthy, and Anderson[4] to investigate stability of the Nagaoka ferromagnetic state. However, since the spin-wave spectrum for general q and finite U derived from Eq. (13), which turns out to be important for our purpose, has not yet been thoroughly investigated, we derive results by ourselves from the outset. Mathematical details are deferred to Appendix B. Below we show only results to compare them with those given in the last subsection.

For the square lattice, the bottom of the continuum $\eta_{\min}(q)=\min_k\eta_q(k)$ and ω_q for $\mathbf{q}=(q,q)$ $(0\leqslant q\leqslant\pi)$ and $U/4t=5$ are shown in Fig. 3, and ω_q for various values of n are shown in Fig. 4.

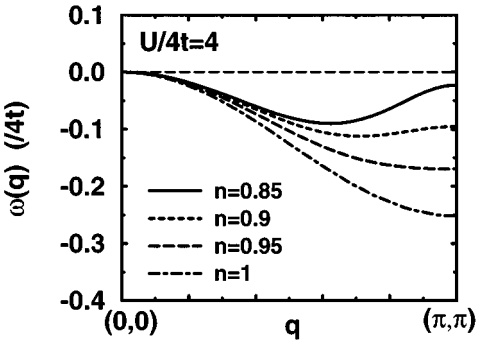

FIG. 4. Dispersion $\omega(q)$ for $U/4t=4$ for the improved trial state.

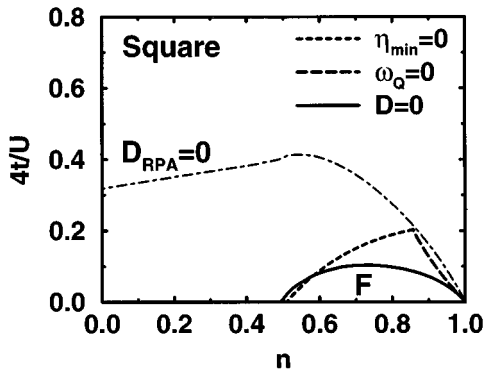

FIG. 5. Threshold for the stability of the ferromagnetic state in a square lattice.

These are to be compared with Fig. 1 and Fig. 2, respectively. As for ω_q, in the slightly doped region $1-n\ll 1$, the results are not modified considerably from those of the RPA. On the other side, the individual particle-hole spectrum presents a striking contrast, as is clear from Fig. 1 and Fig. 3. In the improved estimate, the continuum no longer has energy of order U, but it forms a flat band lying in the low-energy region. This is because of the fact that vacancy made through the hole doping enables particles to hop around, though it is a quite restricted motion.[4] As the density of hole $1-n$ increases, the bandwidth of η_q broadens and finally we have a vanishing binding energy $\Delta_q \equiv \eta_{\min}(q)-\omega_q$ for $q\sim q_{\min}$, as shown in Fig. 3. In the overdoped region, therefore, the spin wave for $q\sim q_{\min}$ cannot be regarded as a well-defined bound state.

III. INSTABILITY OF THE FERROMAGNETIC STATE

A. Hubbard model

In our previous papers,[17,18] we discussed stability of itinerant ferromagnets on the basis of a model comprising degenerate orbitals. In the strong-coupling limit, we observed that the instability condition derived from the individual particle excitation is more stringent than the condition concluded for the spin-wave instability. Therefore, putting more emphasis on the study of the individual particle excitation than for the spin-wave spectrum, we calculated the critical interaction U_c below which excitation energy of the individual particle-hole pair becomes negative as a function of carrier density n.[17] The result for the Hubbard model was that U_c approaches a finite value as $n\to 1$ for both a square and a simple cubic lattice. In other words, we could not prove instability of the Nagaoka ferromagnetic state in the underdoped strong-coupling region, even though a more elaborate trial state than that derived from Eq. (13) is used to estimate energy of the individual-particle excitation. On the contrary, for the Hubbard model, a simple argument can be given, indicating that U_c should become infinity as $n\to 1$. To show this, one may consider the case where holes of concentration $x=1-n$ are doped into the half-filled Hubbard model. If x is small enough, energy of the complete ferromagnetic state is given by $-xzt$ per site. On the other hand, energy of the antiferromagnetic configuration is $-2zt^2/U+O(x)$ per site. Therefore, equating these two, the critical boundary is expected to take the form $zt/U_c \propto x$, as was noted by Nagaoka.[1] This argument, however, does not tell us whether the instability is brought about locally (continuously) or globally. We show that it is in fact given as a local instability by investigating the spin-wave excitation for a strong but finite interaction energy. It is noted here that a quantitative aspect of the above fact was addressed in a recent work by Hanisch, Uhring, and Müller-Hartmann[7] where emphasis is put on how far the stable region of the Nagaoka state can be reduced, rather than its physical origin of our concern.

We display the inverse of the critical coupling as a function of n in Fig. 5 and Fig. 6 for a square and a simple cubic lattice, respectively.[19] In the figures, threshold curves determined using Eq. (13) are shown. These are calculated by the conditions $\eta_{\min}=0$ (dashed), $\omega_Q=0$ (long-dashed), and $D=0$ (solid line), where $\eta_{\min}$ is the minimum value of $\eta_q(k)$. In the region above the curves, the ferromagnetic state is absolutely unstable. Mathematical details for η_q, ω_q, and D are given in Appendix B. The stiffness constant D for the case $zt/U=0$ was shown as a function of n in Ref. 17. In Fig. 5, threshold by $D_{\mathrm{RPA}}=0$ using Eq. (B24) is also shown. It is clear how the trial state (13) improves the result of the RPA; in the latter we cannot prove instability for any n in the strong-coupling region.

The figures show that, in the strong-coupling limit $zt/U=0$, the individual particle excitation (dashed curve) brings about instability prior to the softening of the stiffness

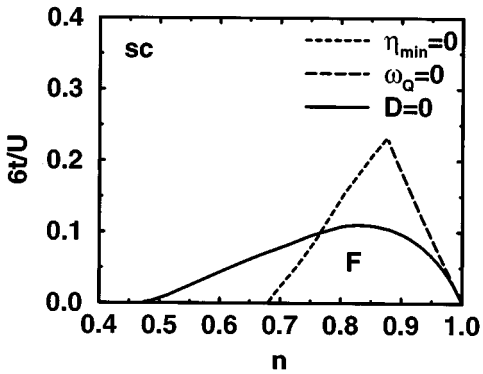

FIG. 6. Threshold for the stability of the ferromagnetic state in a simple cubic lattice.

constant (solid curve), just in accordance with our previous results. However, the phase boundary in the other region is primarily determined by the spin-wave instability, $D<0$. In particular, in the region $U\to\infty$ and $n\to 1$, the phase boundary is of the form $zt/U_c=\kappa x$ and is determined by the spin-wave instability. In this limit, we cannot distinguish the two results by $\omega_Q=0$ and $D=0$, which in turn do not differ appreciably from $D_{\mathrm{RPA}}=0$. Physically we may say that the spin-wave instability determines the threshold for ferromagnetism in the region where the metal-insulator transition is likely to occur. A similar behavior is observed also for the double-exchange ferromagnet as shown in the next subsection.

As for $\kappa\equiv zt/U_c x$, our calculation gives $\kappa=1.08$ for the square lattice ($z=4$). For the simple cubic lattice ($z=6$), we obtained $\kappa=2.08$, which is better than $\kappa=3.96$ of Richmond and Rickayzen,[3] who estimated κ by assuming a flipped spin to stay at a single site, i.e., not to hop around in a lattice as the spin wave does. For reference, we cite Nagaoka's estimate[1] $\kappa=1.47$ for a simple cubic lattice. This value, however, is not to be compared with our result since the former does not have a variational significance. Our result, being based on the variational treatment, sets the exact upper bound for the true value of κ.

B. Double-exchange model

Next, we consider the ferromagnetic Kondo lattice (double exchange) model,

$$H=-t\sum_{i,j,\sigma} c_{i\sigma}^{\dagger}c_{j\sigma}+U\sum_i n_{i\uparrow}n_{i\downarrow}-J'\sum_i \mathbf{S}_{fi}\cdot\mathbf{s}_i + \frac{J'S_f}{2}\sum_{i,\sigma} n_{i\sigma}, \tag{14}$$

where we assume a positive coupling $J'>0$. This model with $S_f=3/2$ is often used to describe the lanthanum manganese oxides $\mathrm{La}_{1-x}A_x\mathrm{MnO}_3$, where A is a divalent ion such as Sr, Pb, or Ca. To create a trial state for the spin-wave excitation, we use the operator

$$b_q^{\dagger}\equiv\frac{1}{\sqrt{L}}\sum_{i,j} f_q(r_j-r_i)[(c_{i\downarrow}^{\dagger}c_{j\uparrow}+S_{fi}^{-})\sin\theta + (c_{i\downarrow}^{\dagger}c_{i\uparrow}+S_{fi}^{-})c_{i\uparrow}^{\dagger}c_{j\uparrow}\cos\theta]e^{iqr_i}, \tag{15}$$

which reduces to Eq. (13) when $S_f=0$. The expression for $\theta=0$, when $U=J'=\infty$, was previously treated by us.[17]

As an example, we show threshold for the instability of the double exchange ferromagnet, the ferromagnetic ground state of Eq. (14). In Fig. 7, we show $6tn/g_c$ determined by $D=0$ as a function of carrier density n (solid curve) where $g\equiv J'S_f+Un$ represents the mean-field exchange splitting of the model (14). We assumed a tight-binding band in a simple cubic lattice. In the figure, we juxtaposed our previous result[17] (dashed curve), which was obtained by investigating the instability of the individual particle excitation; shown as the dashed curve in the right figure of Fig. 9 of Ref. 17. Experimentally, the itinerant ferromagnetic state is observed only in a restricted range $0.2\lesssim x\equiv 1-n\lesssim 0.5$. On the assumption that the model (14) adequately describes the manganese oxides, we may conclude that the observed result is explained by assuming $\overline{U}/6t\equiv g/6tn\sim 5$, i.e., $\overline{U}/W\sim 2.5$ with the bandwidth $W=12t$. In particular, our results indicate the spin-wave instability in the underdoped regime, while in the overdoped regime the instability is controlled by the individual particle excitation with wave number $q\sim k_f$. Generally the spin wave ω_q is made unstable first at the momentum $\mathbf{q}\neq\mathbf{Q}=(\pi,\pi,\pi)$. Therefore the resulting phase beyond the instability is expected to be the incommensurate spiral state,[20] as in the case of the Hubbard model.

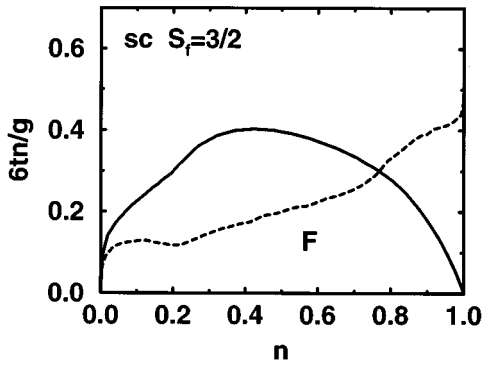

FIG. 7. Inverse of the critical coupling $6tn/g_c$ as a function of n for the $S_f=3/2$ ferromagnetic Kondo lattice model in a simple cubic lattice. The ferromagnetic state is unstable outside the region denoted by F.

In Fig. 8, we show the S_f dependence of the phase boundary $4tn/g$ in a square lattice. Solid curves are determined by $D=0$. As above, for the instability due to the individual-particle excitation (denoted by long-dashed curves), we adopted the more stringent condition $\varepsilon_{k=0\downarrow}=\varepsilon_f$, on the basis of our previous results (7.9) and (7.10) of Ref. 17, than that concluded from the expression derived from Eq. (15), the counterpart of Eq. (B6). The figure shows that the threshold near $n\to 1$ is determined by $D=0$, as in the case of the Hubbard model. The $D=0$ portion of the phase boundary increases as a function of S_f. In particular for $S_f=\infty$ in the

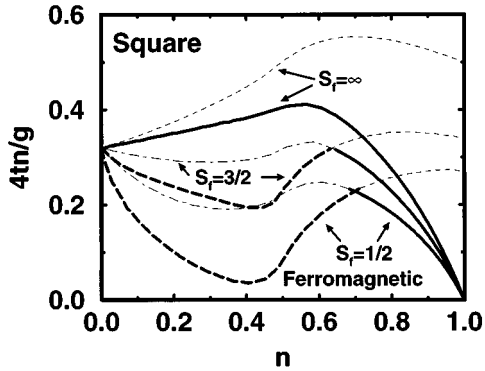

FIG. 8. $4tn/g_c$ as a function of n for the ferromagnetic Kondo lattice model in a square lattice for $S_f=1/2$, 3/2, and ∞. Solid curves are determined by $D=0$. Instability of the individual-particle excitation occurs above the long-dashed curves. The ferromagnetic state is unstable outside the region denoted by ''ferromagnetic.''

square lattice, the boundary is exclusively determined by the condition $D=0$ down to $n=0$, while we found that the solid curve $D=0$ and the dashed curve cross each other around $(n,6tn/g)=(0.5,0.5)$ for $S_f=\infty$ in the simple cubic lattice (not shown in Fig. 7). Note that in the case $S_f=\infty$ the boundary is the same as the result of the random phase approximation. [See $D_{\mathrm{RPA}}=0$ of Fig. 5, as well as Eqs. (B24) and (B25).] We see that all the boundaries in Fig. 8 approach a finite value as $n\to 0$. This is a specific feature of two-dimensional lattices. Generally for $S_f\neq 0$, the parmeter θ in Eq. (15) determined variationally increases from zero to $\pi/2$ as n decreases from 1 to 0. Thus one can show that the condition $D=0$ gives $4tn/g=1/\pi$ in the limit $n\to 0$ for the square lattice, using Eqs. (B24) and (B25). On the other hand, in the simple cubic lattice, we have $1/g\to 0$ in this limit (Fig. 7). Finally we note that the physically relevant situation $S_f=3/2$ lies just in between the classical ($S_f=\infty$) and the quantum ($S_f=1/2$) limit.

IV. DISCUSSION

In the previous section, we showed that the ferromagnetic state in the Hubbard model as well as in the double exchange model is unstable to the spin-wave excitation in the underdoped region, while it is unstable to the individual-particle excitation in the strong-coupling overdoped region. Generally the spin-wave mode ω_q may take a mimimum at finite wave vector $\mathbf{q}=\mathbf{q}_{\min}$. This minimum is interpreted to indicate the potential spiral-spin correlation contained in the ferromagnetic configuration, which becomes conspicuous as the excitation gap $\omega_{q_{\min}}$ approaches zero. We found that the softening of the long-wavelength spin wave mode $D\to 0$ closely follows the gap collapse $\omega_{q_{\min}}\to 0$. Thus we may conclude that the spin-wave instability is a precursor of the metal-insulator transition. It is physically plausible that instability of the ferromagnetic state in the region where the metal-insulator transition is likely to occur is dictated by the spin-wave instability, since the spin wave is nothing but a particle-hole bound state in the ferromagnetic vacuum and, on the other side, we may interpret the Mott insulator as composed of the particle-hole bound states (Appendix A). Therefore we expect that the above conclusion is generally valid; for example, instability of ferromagnetism in the situation appropriate to metallic nickel will be caused by the individual-particle excitation since the filling $n\sim 0.2$ per band is far from being critical for the metal-insulator transition. In this respect, we note that the Hubbard model as a model for an itinerant ferromagnet is a rather exceptional case, because the ferromagnetic state if any can be realized only around half filling (Nagaoka limit). This is the reason why we found a dominant role played by the spin-wave instability in Fig. 5 and Fig. 6.

Finally let us speculate on the approach to the metal-insulator transition from the ferromagnetic side. We could derive the antiferromagnetic Heisenberg model from the spin-wave dispersion of the ferromagnetic insulating state, and observed that, unlike the individual-particle excitation spectrum, the spin-wave dispersion itself does not change drastically upon hole doping (Fig. 1 and Fig. 3). Then if the spin wave as a particle-hole bound state is robust even when a slight amount of holes are doped, the paramagnetic phase realized after the spin-wave instability may show anomalous metallic properties. This kind of consideration makes sense just around half filling only where the lowest energy spin-wave state can be regarded as a well-defined bound state (Fig. 3). Although it is an interesting problem to consider the interacting ferromagnetic spin wave as an elementary constituent, further investigation on this point requires complicated calculation that is far beyond the scope of this article.

ACKNOWLEDGMENTS

The author would like to thank Professor K. Yamada for discussions and critical comments. This work was supported by the Japan Society for the Promotion of Science for Young Scientists.

APPENDIX A: TWO-BODY PROBLEM AND THE HEISENBERG MODEL

Let us consider the simplest case of a particle-hole pair in the ferromagnetic band insulator,

$$|F\rangle\equiv\prod_k c_{k\uparrow}^{\dagger}|0\rangle. \tag{A1}$$

Then the eigenequation for ω_q, which is the eigenvalue of the state (3), is given by

$$\frac{1}{L}\sum_k \frac{1}{\varepsilon_{k+q}-\varepsilon_k+U-\omega_q}=\frac{1}{U}. \tag{A2}$$

This is obtained as a limit $n\to 1$ of Eq. (11), and is the exact result of the two-body problem.[8–11] It is also derived as the condition for the particle-hole ladder to have a pole. We note that the bound-state solution ω_q is nothing but a spin wave in the ferromagnetic vacuum (A1). On the other side, the internal structure of the bound state $f_q(k)$ is given by

$$f_q(k)=\frac{1}{\sqrt{L}}\frac{U}{\varepsilon_{k+q}-\varepsilon_k+U-\omega_q}, \tag{A3}$$

without loss of generality.

We investigate a general case of the tight-binding band, for which ε_k is given by

$$\varepsilon_k=-t\sum_{\overline{\delta}} e^{ik\overline{\delta}}, \tag{A4}$$

where the sum is taken over nearest-neighbor vectors $\overline{\delta}$. To the accuracy of order $O(t/U)$, from Eq. (A2) we obtain an expression for ω_q,

$$\omega_q=-\frac{1}{U}\frac{1}{L}\sum_k (\varepsilon_{k+q}-\varepsilon_k)^2 \tag{A5}$$

$$=-\frac{2t^2}{U}\sum_{\overline{\delta}} (1-e^{iq\overline{\delta}}), \tag{A6}$$

where Eq. (A4) is substituted. The case $n=1$ of Fig. 2 and Fig. 4 can be well fitted by this expression.

As for $f_q(k)$, we have

$$f_q(k)=\frac{1}{\sqrt{L}}\left(1-\frac{\varepsilon_{k+q}-\varepsilon_k}{U}\right), \tag{A7}$$

to the accuracy of order $O(t/U)$. We then obtain

$$f_q(r_j-r_i)=\frac{1}{\sqrt{L}}\sum_k f_q(k)e^{-ik(r_j-r_i)}$$
$$=\delta_{r_j-r_i}+\frac{t}{U}\sum_{\bar{\delta}}\delta_{r_j-r_i-\bar{\delta}}(e^{iq\bar{\delta}}-1), \tag{A8}$$

and

$$b_i^\dagger=\frac{1}{\sqrt{L}}\sum_q b_q^\dagger e^{-iqr_i}$$
$$=\frac{1}{L}\sum_q\sum_{i',j'} f_q(r_{j'}-r_{i'})c_{i'\downarrow}^\dagger c_{j'\uparrow}e^{iq(r_{i'}-r_i)}$$
$$=c_{i\downarrow}^\dagger c_{i\uparrow}+\frac{t}{U}\sum_{\bar{\delta}}(c_{i-\bar{\delta}\downarrow}^\dagger c_{i\uparrow}-c_{i\downarrow}^\dagger c_{i+\bar{\delta}\uparrow}). \tag{A9}$$

The result Eq. (A9) shows that the boson $b_i^\dagger$ for nonzero t/U has an internal structure extending to neighboring sites of the site where it is created. Physically this structure is interpreted as a singlet cloud formed with the neighboring sites.

Energy of the localized boson is given by

$$\omega_i=\frac{\langle F|b_i[H,b_i^\dagger]|F\rangle}{\langle F|b_ib_i^\dagger|F\rangle}=-\frac{2zt^2}{U}, \tag{A10}$$

where z is a coordination number, $z=\sum_{\bar{\delta}}1$. The result Eq. (A10) is obtained also as the center of gravity of the band ω_q, Eq. (A6),

$$\bar{\omega}_q=\frac{1}{L}\sum_q \omega_q=-\frac{2zt^2}{U}. \tag{A11}$$

From the form of the structure, Eq. (A9), Eq. (A10) is interpreted as a sum of energy of singlets formed with the z nearest neighbors. The factor 2 is due to the two processes due to a particle and a hole hopping, which are represented in the two terms in the parentheses of Eq. (A9).

Now let us introduce the creation and annihilation operator of the hard-core boson $\tilde{b}_i^\dagger$ and $\tilde{b}_i$ in place of $b_i^\dagger$ and b_i;

$$b_i^\dagger\to\tilde{b}_i^\dagger, \quad b_i\to\tilde{b}_i. \tag{A12}$$

The bound state created by $b_i^\dagger$ extends only to the nearest-neighboring sites of i, as indicated from Eq. (A9). As a result, total energy of two localized bosons differs from $2\omega_i$ only when they are in the nearest-neighboring sites, when the total energy amounts to $-4(z-1)t^2/U$. Increase by an amount $2J\equiv 4t^2/U$ from $2\omega_i$ is due to overlap of the singlet cloud of the two bosons. In the hard-core boson picture this must be regarded as an interaction energy, i.e., the interaction part of the Hamiltonian for the hard-core boson is given by

$$\tilde{V}=2J\sum_{\langle i,j\rangle}\tilde{b}_i^\dagger\tilde{b}_i\tilde{b}_j^\dagger\tilde{b}_j, \tag{A13}$$

where the sum is taken over the nearest-neighbor pairs. On the other side for the hopping part, the one-body energy ω_q is given by Eq. (A6). In terms of $J\equiv 2t^2/U$ we rewrite it as

$$\tilde{T}=\sum_q \omega_q\tilde{b}_q^\dagger\tilde{b}_q=-J\sum_q\sum_{\bar{\delta}}(1-e^{iq\bar{\delta}})\tilde{b}_q^\dagger\tilde{b}_q$$
$$=J\sum_{\langle i,j\rangle}(-\tilde{b}_i^\dagger\tilde{b}_i-\tilde{b}_j^\dagger\tilde{b}_j+\tilde{b}_i\tilde{b}_j^\dagger+\tilde{b}_i^\dagger\tilde{b}_j). \tag{A14}$$

Instead of the hard-core boson, we can equivalently use the quantum operator for the spin $S=1/2$, which are defined by

$$S_{zi}=\tfrac{1}{2}-\tilde{b}_i^\dagger\tilde{b}_i,$$
$$S_i^+=\tilde{b}_i, \quad S_i^-=\tilde{b}_i^\dagger. \tag{A15}$$

Then as the effective model to describe the half-filled Hubbard model in the strong-coupling regime, we can reproduce the antiferromagnetic Heisenberg model in terms of these spin operators: Putting Eq. (A13) and Eq. (A14) together, we obtain

$$\tilde{H}=\tilde{T}+\tilde{V}=2J\sum_{\langle i,j\rangle}[(\tfrac{1}{2}-\tilde{b}_i^\dagger\tilde{b}_i)(\tfrac{1}{2}-\tilde{b}_j^\dagger\tilde{b}_j)$$
$$+\tfrac{1}{2}(\tilde{b}_i\tilde{b}_j^\dagger+\tilde{b}_i^\dagger\tilde{b}_j)-\tfrac{1}{4}]$$
$$=2J\sum_{\langle i,j\rangle}[S_{zi}S_{zj}+\tfrac{1}{2}(S_i^+S_j^-+S_i^-S_j^+)-\tfrac{1}{4}]$$
$$=2J\sum_{\langle i,j\rangle}(\mathbf{S}_i\cdot\mathbf{S}_j-\tfrac{1}{4}). \tag{A16}$$

Similarly as above, as an effective model for the case when holes are doped, the following Hamiltonian is suggested:

$$H=t\sum_{i,j}\tilde{f}_i^\dagger\tilde{f}_j-t\sum_{i,j}\tilde{b}_i^\dagger\tilde{f}_i\tilde{f}_j^\dagger\tilde{b}_j+2J\sum_{\langle i,j\rangle}(\mathbf{S}_i\cdot\mathbf{S}_j-\tfrac{1}{4}). \tag{A17}$$

The first term describes the hopping process of a doped hole, $\tilde{f}_i^\dagger\equiv c_{i\uparrow}(1-\tilde{b}_i^\dagger\tilde{b}_i)$, and the second term takes into account the hopping of the boson when its neighboring sites are vacant. The Hilbert space of Eq. (A17) is spanned at each site by $|\uparrow_i\rangle$, $|\downarrow_i\rangle\equiv\tilde{b}_i^\dagger|\uparrow_i\rangle$ and vacancy $|0_i\rangle\equiv\tilde{c}_{i\uparrow}|\uparrow_i\rangle$. The fermion operator $\tilde{c}_{i\uparrow}$ must thus be operated on the sites where there is no boson. To take this into account, one may use $\tilde{f}_i^\dagger$ instead of $\tilde{c}_{i\uparrow}$.

APPENDIX B: CALCULATION FOR THE IMPROVED VARIATIONAL STATE

We calculate ω_q for the creation operator,

$$b_q^\dagger \equiv \frac{1}{\sqrt{L}}\sum_{i,j}\ [f_q(r_j-r_i)c_{i\downarrow}^\dagger c_{j\uparrow}+\overline{f_q}(r_j-r_i)c_{i\downarrow}^\dagger c_{i\uparrow}^\dagger c_{j\uparrow}]e^{iqr_i}. \tag{B1}$$

To obtain results, we may follow the same procedure as given in Sec. II A. First we obtain

$$\langle F|b_q[H,b_q^\dagger]|F\rangle=\frac{1}{L}\sum_k\ n_k(\varepsilon_{k+q}-\varepsilon_k+Un)|f_k|^2-U\left|\frac{1}{L}\sum_k\ n_k f_k\right|^2+\frac{1}{L}\sum_k\ \Delta_{kq}|\overline{f_k}|^2+\frac{1}{L^2}\sum_{k,p}\ \Gamma_{kpq}\overline{f_k^*}\,\overline{f_p}$$
$$+\left(\frac{1}{L}\sum_k\ n_k(\varepsilon_{k+q}-\varepsilon_k)\,\overline{f_k^*}\right)\left(\frac{1}{L}\sum_k\ n_k f_k\right)+\begin{bmatrix}\overline{f_k^*}\to f_k^*\\ f_k\to\overline{f_k}\end{bmatrix}+\frac{1-n}{L}\sum_k\ n_k(\varepsilon_{k+q}-\varepsilon_k)\,\overline{f_k^*}f_k+\begin{bmatrix}\overline{f_k^*}\to f_k^*\\ f_k\to\overline{f_k}\end{bmatrix}, \tag{B2}$$

and

$$\langle F|b_q b_q^\dagger|F\rangle=\frac{1}{L}\sum_k\ n_k|f_k|^2+\frac{1-n}{L}\sum_k\ |\overline{f_k}|^2+\left|\frac{1}{L}\sum_k\ n_k\overline{f_k}\right|^2+\left(\frac{1}{L}\sum_k\ n_k\overline{f_k^*}\right)\left(\frac{1}{L}\sum_k\ n_k f_k\right)+\begin{bmatrix}\overline{f_k^*}\to f_k^*\\ f_k\to\overline{f_k}\end{bmatrix}$$
$$+\frac{1-n}{L}\sum_k\ n_k\overline{f_k^*}f_k+\begin{bmatrix}\overline{f_k^*}\to f_k^*\\ f_k\to\overline{f_k}\end{bmatrix}. \tag{B3}$$

Here we denoted $f_q(k)$ simply as f_k. Bracketed expressions mean to repeat the preceding terms with the replaced functions as indicated in the brackets. Δ_{kq} and Γ_{kpq} in Eq. (B2) is the case $S_f=0$ of the expression defined in (4.6) and (4.7) of Ref. 17. In the tight-binding dispersion Eq. (A4), the former is given by

$$\Delta_{kq}=|\epsilon_g|-(1-n)\varepsilon_k+\left((1-n)^2-\left|\frac{\epsilon_g}{zt}\right|^2\right)\varepsilon_{k+q}, \tag{B4}$$

where

$$\epsilon_g\equiv\frac{1}{L}\sum_k\ n_k\varepsilon_k. \tag{B5}$$

For the wave function Eq. (13), one may replace f_k and $\overline{f_k}$ in the above expressions by $f_k\sin\theta$ and $f_k\cos\theta$, respectively. A function f_k and a parameter θ have to be fixed so as to minimize ω_q. We note that Eq. (13) for $\theta=\pi/2$ gives Eq. (4). Moreover, Eq. (13) becomes the trial state for the case $U=\infty$ (Refs. 2 and 4) by assuming $\theta=0$, since in this case the variational state does not depend on the interaction energy U at all. For a finite value of U, the parameter θ takes a value in the range $0\leqslant\theta\leqslant\pi/2$.

1. Individual particle excitation

To derive excitation energy of the individual particle-hole pair, we may set $f_{k'}=\delta_{kk'}$ in Eqs. (B2) and (B3) to calculate

$$\omega_q=\frac{\langle F|b_q[H,b_q^\dagger]|F\rangle}{\langle F|b_q b_q^\dagger|F\rangle}.$$

Then we obtain

$$\eta_q(k,\theta)=\frac{\Delta_{kq}\cos^2\theta+(\varepsilon_{k+q}-\varepsilon_k+Un)\sin^2\theta+2(1-n)(\varepsilon_{k+q}-\varepsilon_k)\sin\theta\cos\theta}{(1-n)\cos^2\theta+2(1-n)\sin\theta\cos\theta+\sin^2\theta}. \tag{B6}$$

For $\eta_q(k)$ this expression should be minimized with respect to θ, and $\eta_{\min}$ is defined as a minimum of $\eta_q(k)$.

2. Spin-wave dispersion

To minimize ω_q with respect to f_k, we take functional derivative $\partial\omega_q/\partial f_p^*$ after replacing f_k and $\overline{f_k}$ in Eqs. (B2) and (B3) by $f_k\sin\theta$ and $f_k\cos\theta$. Then we obtain an equation,

$$\left(\Delta_{kq}f_k+\frac{1}{L}\sum_p\ \Gamma_{kpq}f_p\right)\cos^2\theta+\left((\varepsilon_{k+q}-\varepsilon_k+Un)f_k-\frac{U}{L}\sum_k\ n_k f_k\right)\sin^2\theta+\left(\frac{\varepsilon_{k+q}-\varepsilon_k}{L}\sum_k\ n_k f_k+\frac{1}{L}\sum_k\ n_k(\varepsilon_{k+q}-\varepsilon_k)f_k\right.$$
$$\left.+2(1-n)(\varepsilon_{k+q}-\varepsilon_k)f_k\right)\sin\theta\cos\theta=\omega_q\left[\left((1-n)f_k+\frac{1}{L}\sum_k\ n_k f_k\right)\cos^2\theta+f_k\sin^2\theta+\left(\frac{2}{L}\sum_k\ n_k f_k+2(1-n)f_k\right)\sin\theta\cos\theta\right]. \tag{B7}$$

We investigate the tight-binding model in a square ($d=2$) and simple cubic lattice ($d=3$), for which

$$\varepsilon_k=-\frac{1}{d}\sum_{i=1}^{d}\cos(k_i). \tag{B8}$$

Here and below we set $zt=1$ where $z=2d$. Furthermore, we are interested in the dispersion ω_q for q along the diagonal of the Brillouin zone, i.e., for $\mathbf{q}=(q,q)$ and $\mathbf{q}=(q,q,q)$ $(0\leqslant q\leqslant\pi)$ in the square and the simple cubic lattice, respectively. Then we can cast Eq. (B7) into the following form:

$$D(k,q)f_q(k)=\sum_{i=1}^{3}N_i(k,q)F_i(q), \tag{B9}$$

where

$$D(k,q)=[\Delta_{kq}-(1-n)\omega_q]\cos^2\theta+(\varepsilon_{k+q}-\varepsilon_k+Un-\omega_q)\times\sin^2\theta+2(1-n)(\varepsilon_{k+q}-\varepsilon_k-\omega_q)\sin\theta\cos\theta, \tag{B10}$$

$$F_i(q)\equiv\frac{1}{L}\sum_k n_k(\delta_{i1}-\varepsilon_k\delta_{i2}+\tilde{\varepsilon}_k\delta_{i3})f_q(k), \tag{B11}$$

$$N_1(k,q)\equiv[\omega_q-|\epsilon_g|\varepsilon_q-(1-n)\varepsilon_{k+q}]\cos^2\theta+U\sin^2\theta+(2\omega_q-\varepsilon_{k+q}+\varepsilon_k)\sin\theta\cos\theta, \tag{B12}$$

$$N_2(k,q)\equiv-[|\epsilon_g|\varepsilon_{k+q}+(1-n)\varepsilon_q]\cos^2\theta-(1+\varepsilon_q)\sin\theta\cos\theta, \tag{B13}$$

$$N_3(k,q)\equiv-[|\epsilon_g|\tilde{\varepsilon}_{k+q}+(1-n)\tilde{\varepsilon}_q]\cos^2\theta-v_q\sin\theta\cos\theta. \tag{B14}$$

Here we introduced

$$\tilde{\varepsilon}_k=\frac{1}{d}\sum_{i=1}^{d}\sin(k_i),\quad v_q=\sin(q). \tag{B15}$$

Solving Eq. (B9) for $f_q(k)$ and substituting the result into Eq. (B11), we get the eigenequation

$$\det[A_{ij}(q)-\delta_{ij}]=0, \tag{B16}$$

where

$$A_{ij}(q)=\frac{1}{L}\sum_k n_k(\delta_{i1}-\varepsilon_k\delta_{i2}+\tilde{\varepsilon}_k\delta_{i3})\frac{N_j(k,q)}{D(k,q)}. \tag{B17}$$

To obtain the spin-wave energy ω_q, we must minimize the solution $\omega_q(\theta)$ of Eq. (B16) with respect to θ.

3. Spin-wave stiffness constant

The spin-wave stiffness constant D is defined by

$$\omega_q=Dq^2\quad(q\to0). \tag{B18}$$

In the long-wavelength limit $q\to0$, we can expand $f_q(k)$ with respect to q and derive D analytically from Eq. (B2) and Eq. (B3). Below we give only the resulting expressions.

As shown in our previous paper,[17] the results for the Hubbard model are obtained as a special case of those for the Kondo lattice model (14). Using Eq. (15), we calculated D for this general model;

$$D(\theta)=D_0-\delta D(\theta), \tag{B19}$$

where $D_0=|\epsilon_g|/2Sz$ in terms of twice the spontaneous magnetization $2S\equiv2S_f+n$, and

$$\delta D(\theta)=\frac{I((1-n)\cos^2\theta+\sin^2\theta+(2-n)\sin\theta\cos\theta)^2}{2S(1+|\epsilon_g|zI\cos^2\theta/2)(1+2\sin\theta\cos\theta)}\quad(>0). \tag{B20}$$

In these expressions, I, v_{k_x}, and Δ_{k0} are given by

$$I=\frac{1}{L}\sum_k\frac{n_k v_{k_x}^2}{\Delta_{k0}\cos^2\theta+g\sin^2\theta}, \tag{B21}$$

$$v_{k_x}=\frac{\partial\varepsilon_k}{\partial k_x}, \tag{B22}$$

and

$$\Delta_{k0}=(2S_f+1)[|\epsilon_g|-(1-n)\varepsilon_k]+[(1-n)^2-|\epsilon_g|^2]\varepsilon_k\quad(>0). \tag{B23}$$

A parameter g in Eq. (B21) is defined by $g=Un+J'S_f$, and represents the mean-field exchange splitting of the model (14). We must minimize $D(\theta)$ to obtain D. To reproduce the result for the Hubbard model, we may set $S_f=0$. The particular case of the above results, i.e., in the strong-coupling limit $g=\infty$ $(\theta=0)$, was obtained previously.[4,17] For the Hubbard model, the result of the random phase approximation D_{RPA} is obtained by setting $S_f=0$ and $\theta=\pi/2$,

$$D_{\mathrm{RPA}}=\frac{|\epsilon_g|}{zn}-\frac{1}{Un^2}\frac{1}{L}\sum_k n_k v_{k_x}^2. \tag{B24}$$

A similar expression is obtained in the limit $S\to\infty$ where we should assume $\theta=\pi/2$ to keep I and $2S\,\delta D(\theta)$ finite. Then we obtain

$$D_{S\to\infty}=\frac{1}{2S}\left(\frac{|\epsilon_g|}{z}-\frac{1}{g}\frac{1}{L}\sum_k n_k v_{k_x}^2\right). \tag{B25}$$

In the main text, we regarded the approximation scheme giving the result corresponding to Eqs. (B24) and (B25) as the random phase approximation. The former result (B24) is well known for the Hubbard model. The latter was recently obtained by another method.[21]

[1] Y. Nagaoka, Phys. Rev. **147**, 392 (1966).
[2] L. M. Roth, J. Phys. Chem. Solids **28**, 1549 (1967); J. Appl. Phys. **39**, 474 (1968).
[3] P. Richmond and G. Rickayzen, J. Phys. C **2**, 528 (1969).
[4] B. S. Shastry, H. R. Krishnamurthy, and P. W. Anderson, Phys. Rev. B **41**, 2375 (1990).
[5] A. G. Basile and V. Esler, Phys. Rev. B **41**, 4842 (1990).
[6] W. von der Linden and D. M. Edwards, J. Phys.: Condens. Matter **3**, 4917 (1991).
[7] T. Hanisch, G. S. Uhrig, and E. Müller-Hartmann, Phys. Rev. B **56**, 13 960 (1997). 1997).
[8] W. Kohn, Phys. Rev. **133**, A171 (1964).
[9] K. Dichtel, R. J. Jelitto, and H. Koppe, Z. Phys. B **246**, 248 (1971).
[10] Q. P. Li and R. Joynt, Phys. Rev. B **47**, 3979 (1993); **49**, 1632 (1994).
[11] P. G. J. van Dongen and V. Janiš, Phys. Rev. Lett. **72**, 3258 (1994).
[12] K. Dichtel, R. J. Jelitto, and H. Koppe, Z. Phys. B **251**, 173 (1972).
[13] H. R. Krishnamurthy, C. Jayaprakash, S. Sarker, and W. Wenzel, Phys. Rev. Lett. **64**, 950 (1990); S. Sarker, C. Jayaprakash, H. R. Krishnamurthy, and W. Wenzel, Phys. Rev. B **43**, 8775 (1991); C. Jayaprakash, H. R. Krishnamurthy, S. Sarker, and W. Wenzel, Europhys. Lett. **15**, 625 (1991).
[14] B. I. Shraiman and E. D. Siggia, Phys. Rev. Lett. **62**, 1564 (1989).
[15] C. Jayaprakash, H. R. Krishnamurthy, and S. Sarker, Phys. Rev. B **40**, 2610 (1989).
[16] D. Yoshioka, J. Phys. Soc. Jpn. **58**, 1516 (1989).
[17] T. Okabe, Prog. Theor. Phys. **97**, 21 (1997); **97**, 559 (1997).
[18] T. Okabe, Prog. Theor. Phys. **98**, 331 (1997).
[19] The same kind of phase diagram was given in Ref. 4, where the result of Ref. 3 had to be cited to supplement the portion $zt/U_c \propto x$ for $U \to \infty$ and $x \to 0$.
[20] J. Inoue and S. Maekawa, Phys. Rev. Lett. **74**, 3407 (1995).
[21] N. Furukawa, J. Phys. Soc. Jpn. **65**, 1174 (1996).